



Dalton  
Transactions

**A novel symmetric pyrazine (pyz)-bridged uranyl dimer  
[UO<sub>2</sub>Cl<sub>3</sub>(H<sub>2</sub>O)(Pyz)<sub>0.5</sub>]<sub>2</sub><sup>2-</sup>: Synthesis, structural and  
computational analysis**

Journal:	<i>Dalton Transactions</i>
Manuscript ID	DT-ART-05-2022-001486.R1
Article Type:	Paper
Date Submitted by the Author:	23-Jun-2022
Complete List of Authors:	Byrne, Nicole; The George Washington University, Chemistry Schofield, Mark; The George Washington University, Chemistry Cahill, Chris; The George Washington University, Chemistry

SCHOLARONE™  
Manuscripts

## A novel symmetric pyrazine (pyz)-bridged uranyl dimer $[\text{UO}_2\text{Cl}_3(\text{H}_2\text{O})(\text{Pyz})_{0.5}]_2^{2-}$ : Synthesis, structural and computational analysis

Nicole M. Byrne,<sup>a</sup> Mark H. Schofield,<sup>a</sup> Christopher L. Cahill<sup>a\*</sup>

<sup>a</sup>Department of Chemistry, The George Washington University, 800 22<sup>nd</sup> St. NW, Suite 4000, Washington, D.C., 20052

### Abstract

Herein we report on the synthesis of  $(\text{HPyz}^+)_2[\text{UO}_2\text{Cl}_3(\text{H}_2\text{O})(\text{Pyz})_{0.5}]_2 \cdot 2\text{H}_2\text{O}$  which features a novel pyrazine-bridged uranyl dimer,  $[\text{UO}_2\text{Cl}_3(\text{H}_2\text{O})(\text{Pyz})_{0.5}]_2^{2-}$ . A rigorous computational and experimental analysis of this compound was performed to fully explore the influence of coordination on the electronic structure and potential charge-transfer characteristics of this dimer, revealing a delocalized  $\pi$ -system across the bridging pyrazine and the axial components of both uranyl centers. Electrostatic surface potentials, used to rationalize the observed assembly, indicate a decreased basicity of the uranyl oxo versus  $[\text{UO}_2\text{Cl}_4]^{2-}$ , and signify a lessened capacity for the terminal -yl oxos of the  $[\text{UO}_2\text{Cl}_3(\text{H}_2\text{O})(\text{Pyz})_{0.5}]_2^{2-}$  dimer to participate in supramolecular assembly. A combined density functional theory (DFT) and quantum theory of atoms in molecules (QTAIM) analysis further evidenced an increase in U=O bond strengths within the dimer, which is supported by a blue shift in the characteristic Raman-active uranyl symmetric stretch ( $\nu_1$ ) with respect to the more typically observed  $[\text{UO}_2\text{Cl}_4]^{2-}$ .

## Introduction

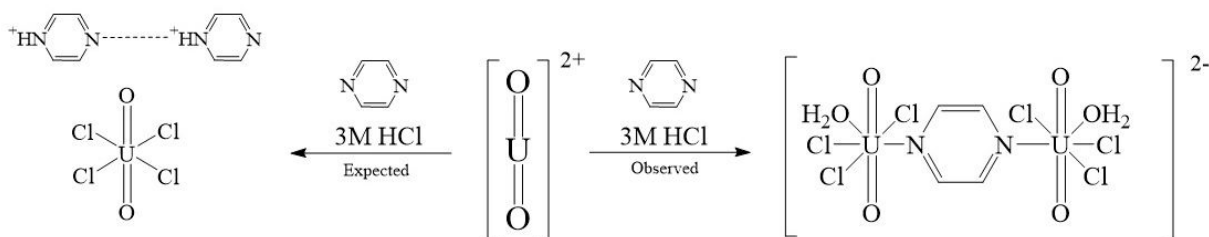
Directed assembly of reproducible inorganic anions with organic cations has proven useful for studying restricted speciation profiles in solution and, in turn, control over the solid products formed.<sup>1-9</sup> As such, we have a particular interest in the role of second-sphere interactions in the assembly process and the resultant effect on spectroscopic properties of uranyl containing solid-state materials. Our group<sup>1-4,10</sup> and others<sup>5-8,11,12</sup> have previously reported on the use of a robust synthetic strategy, using a combination of low pH and high anion media, as a means to offset uranyl hydrolysis and control assembly. In this way, one may reliably produce the  $[\text{UO}_2\text{X}_4]^{2-}$  (X = Cl, Br) building unit paired with a suite of organic cations. We attempted to utilize this synthetic strategy to pair the uranyl tetrachloride dianion with a pyrazinium cation, with the aim of probing structure-property relationships. Typical compounds of this type pair the  $[\text{UO}_2\text{Cl}_4]^{2-}$  with protonated organic cations via hydrogen bonding to one another.<sup>3,8,13</sup> The resultant phase from our current efforts, however, afforded a novel  $[\text{UO}_2\text{Cl}_3(\text{H}_2\text{O})(\text{Pyz})_{0.5}]_2^{2-}$  *dimer*, which highlights an intriguing divergence from the often-observed tetrahalide monomer and expected protonation of the pyrazine. As such, we have been afforded a platform for probing bonding and electronic structure in a novel coordination geometry for the uranyl cation.

Transition metal complexes featuring pyrazine bridges have been well-studied, often exhibiting strong charge-transfer properties and their ability to stabilize half integer oxidation states in mixed-valent species.<sup>14-19</sup> In such compounds, work has been done to prove delocalization of the electron cloud about the pyrazine ring, which is thereby responsible for their strong electron transfer characteristics. Desired characteristics from these compounds stem from typically being bimetallic and/or mixed valent, such as the Creutz-Taube ion,<sup>14-16,18</sup> which allows for delocalization of electron density among the metal centers. Much work has been done to

characterize these phases, including crystallography, spectroscopy, and density functional theory calculations, with hopes of gaining a holistic picture of the properties and electronic structure. Mehdoui *et al.* previously attempted to prepare a U(III)/U(IV) mixed-valent couple of this type, however the strong  $\pi$  donation from the metal to pyrazine  $\pi^*$  orbitals led to U(III) oxidation, resulting in a homovalent U(IV) phase.<sup>20</sup> Whereas the coordination chemistry of actinide complexes is indeed quite rich and features many examples of dimeric complexes with various oxidation states and bearing bridging ligands (**SI Chart S1**), it is interesting to note compound **1** represents the first U(VI) actinyl example of a discrete, pyrazine bridged dimer. Moreover, we note the resemblance to a homovalent Creutz-Taube ion. As such, **1** merited a comprehensive experimental and computational treatment to probe the influence of the pyrazine bridge on electronic structure and uranium-ligand bonding as we deviate from the typically observed  $[\text{UO}_2\text{Cl}_4]^{2-}$  anion to this dimer. To this end, we have performed a robust density functional theory (DFT) and Bader's Quantum Theory of Atoms in Molecules (QTAIM) treatment, in addition to Raman, luminescence and diffuse reflectance spectroscopy, in order to probe the nature of electronic structure and bonding in this phase.

## Experimental Methods

**Synthesis:** *Caution!* Although the uranium source used (uranyl acetate dihydrate  $[\text{UO}_2(\text{CH}_3\text{COO})_2] \cdot 2\text{H}_2\text{O}$ ) contains depleted uranium, precautions for handling radioactive materials should be followed. Uranyl acetate dihydrate (Fisher Scientific, 99%), pyrazine (99+%, Aldrich) and ACS reagent grade HCl (Sigma Aldrich, 37%), are all commercially available and were used without further purification prior to synthesis.



**Scheme 1:** Expected versus observed assembly of **1**. In the middle, is the bare uranyl cation (solvent excluded for clarity) flanked by the expected and observed assembly pathways. (Left): Expected uranyl tetrachloride anion, exhibiting square bipyramidal geometry of the uranyl cation with 4 chlorides in the equatorial plane. Pyrazine present is of the monovalent pyrazinium form, hydrogen bonding to one another. (Right): Observed uranyl dimeric anion, with the pyrazine bridging the two metal centers, each flanked by three additional chlorides and a water equatorially.

A combination of low pH and high anion media was used to minimize hydrolysis of the uranyl cation in aqueous solution and limit solid-state speciation. Uranyl acetate dihydrate (0.025 g, 0.059 mmol) was dissolved in 5 mL 3M HCl in a 2 dram glass scintillation vial. To this, 3 molar equivalents (0.014 g, 0.177 mmol) of pyrazine were added. The resultant clear, yellow solution was allowed to slowly evaporate in ambient conditions until reaching dryness, which took approximately one month. The resultant crystals are prone to rapid degradation and do not survive long once removed from their mother liquor.

**Single Crystal X-ray Diffraction:** A single crystal of the title compound was selected and mounted on a 20  $\mu\text{m}$  MiTeGen micromount. XRD data was collected on a Bruker D8 Quest equipped with a Photon II detector, utilizing a Mo  $K\alpha$  x-ray source. Reflections were collected using  $0.5^\circ$   $\omega$  and  $\varphi$  scans at 100(2) K. APEX III software was used to analyze and integrate the data,<sup>21</sup> as well as perform an absorption correction *via* SAINT,<sup>22</sup> with structure solutions by direct methods using SHELXL-16.<sup>23,24</sup> The WinGx software suite was then used for structural refinements.<sup>25</sup> All non-hydrogen atoms were refined anisotropically after being located on Fourier difference maps. Hydrogen atoms were then placed using HFIX commands, which allow hydrogen

atoms to refine off of their parent atoms. After final refinement, images for publication were generated using CrystalMaker 8.2.2.<sup>26</sup>

**Spectroscopy:** Diffuse reflectance spectroscopy was performed on isolated single crystals, using a Mikropack DH-2000-BAL deuterium and halogen light source coupled via fiber optics to an Ocean Optics Flame Detector. Prior to collection, BaSO<sub>4</sub> was used as a reference for calibration. Data was then processed using the OceanView software. Luminescence spectra were collected at both 298 and 78 K, using a Horiba Fluorolog-3 spectrophotometer, which incorporates a 450 W xenon arc lamp with double excitation and double emission monochromators. A 950 V photomultiplier tube was used as the detector. Sample was housed on a quartz plate held within a Janis VPF-100 cryostat for measurements, which is equipped with UV-grade fused silica windows. To control for temperature, a Lakeshore model 325 temperature controller was used. Raman spectroscopy of single crystals were collected on a Horiba LabRam HR Evolution Raman Microscope over the 200-2000 cm<sup>-1</sup> range. Excitation was performed using a 532 cm<sup>-1</sup> light source, at 2 seconds with 20 accumulations.

**Computational Analysis:** Density functional theory (DFT) calculations were performed utilizing Gaussian16<sup>27</sup> in combination with NBO7.<sup>28</sup> Frequency, wavefunction, and NBO analyses were performed using the B3LYP functional<sup>29,30</sup> with the def2TZVP basis set for O, N, Cl, C, and H, and ECP60MWB and ECP60MWB-SEG pseudopotential for U.<sup>31,32</sup> Atomic coordinates for the [UO<sub>2</sub>Cl<sub>3</sub>(H<sub>2</sub>O)(Pyz)<sub>0.5</sub>]<sub>2</sub><sup>2-</sup> model were extracted directly from the .cif for compound **1**, with those for [UO<sub>2</sub>Cl<sub>4</sub>]<sup>2-</sup> taken from (C<sub>6</sub>H<sub>8</sub>N)<sub>2</sub>[UO<sub>2</sub>Cl<sub>4</sub>],<sup>3</sup> to serve as a reference compound in discussion of the U=O bond, and was given identical treatment to **1**. Said models were treated with a GD3BJ empirical dispersion correction,<sup>33,34</sup> and were treated as single-point energy calculations without optimization. Outputs from these calculations were used to produce electrostatic surface potentials

(ESPs), render HOMO and LUMO orbitals, Natural Localized Molecular Orbital (NLMO) analysis, Wiberg bond indices, and quantum theory of atoms in molecules (QTAIM) analysis. In order to best reflect accurate group theory in our vibrational analyses, and minimize the impact of negative and/or imaginary frequencies, an optimization step was included for this step only. While the geometry optimized structure differs only minimally from x-ray diffraction atomic coordinates, and is more appropriate for vibrational analysis, canting of both the bridging pyrazine ring and equatorial water molecules introduces several bonds not present in the unoptimized model, and as such, was not used to reflect bonding in our models (**SI Figure S5**). All calculations were validated across several functionals including BLYP, CAM-B3LYP, BP86, PBE1PBE, and TPSSH (**SI Table S5 and S6**). Electrostatic surface potential (ESP) maps generated at a 0.002 isovalue, in addition to vibrational modes (**SI GIFs 1-3**), were rendered in GaussView 6.0.<sup>35</sup> Visualization of HOMO and LUMO orbitals was performed in Avogadro.<sup>36,37</sup> The wavefunctions from the B3LYP calculations were used to perform Bader's Quantum Theory of Atoms in Molecules (QTAIM)<sup>38</sup> analysis using AIMAll.<sup>39,40</sup> Resultant outputs from this calculation were then rendered and analyzed using AimStudio.

## Results

**Structural description (HPyz<sup>+</sup>)<sub>2</sub>[UO<sub>2</sub>Cl<sub>3</sub>(H<sub>2</sub>O)(Pyz)<sub>0.5</sub>]<sub>2</sub>·2H<sub>2</sub>O:** Compound **1** crystallizes in the space group P-1, and features a novel [UO<sub>2</sub>Cl<sub>3</sub>(H<sub>2</sub>O)(Pyz)<sub>0.5</sub>]<sub>2</sub><sup>2-</sup> dimer charge balanced by lattice pyrazinium cations. The dimer consists of two crystallographically unique uranyl centers each bound by three chlorides and a water. The two metal centers are then bridged by an N-bound pyrazine which lays perpendicular to the equatorial plane. The dimer participates in two equivalent hydrogen bonds between the isolated equatorial chloride and water with those on an adjacent anion

( $d_{\text{Cl}\dots\text{OH}_2} = 3.158(2) \text{ \AA}$ ,  $\text{vdW}\% = 96.6\%$ )<sup>41</sup> which forms chains down the *b*-axis (**Figure 1**). One of the remaining equatorial chlorides participates in hydrogen bonding with a lattice water ( $d_{\text{Cl}\dots\text{OH}_2} = 3.198(2) \text{ \AA}$ ,  $\text{vdW}\%_1 = 97.8\%$ ). The uranyl oxo also exhibits oxo- $\pi$  interactions ( $d_{\text{pyz}\dots\text{oxo}} = 3.662 \text{ \AA}$ ) with a lattice pyrazine. There are no other meaningful interactions to the dimer to report. There are also hydrogen bonds between lattice pyrazinium and water molecules ( $d_{\text{pyz}^+\dots\text{OH}_2} = 2.693(3) \text{ \AA}$ ,  $\text{vdW}\% = 87.7\%$ ).

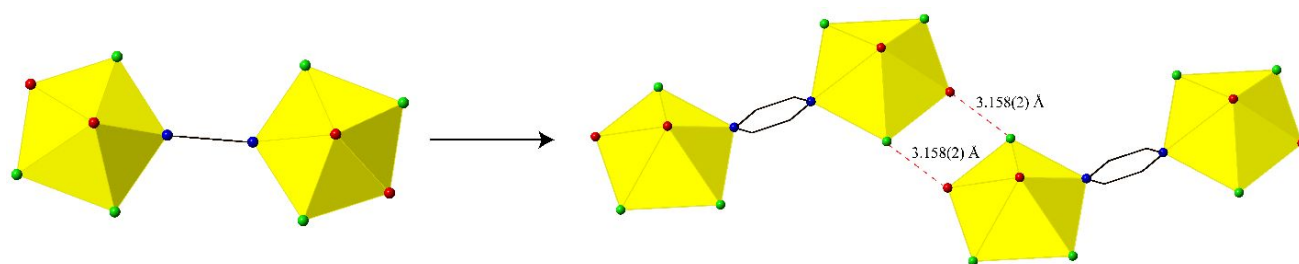


**Figure 1:** (Left): Representative  $[\text{UO}_2\text{Cl}_3(\text{H}_2\text{O})(\text{Pyz})_{0.5}]_2^{2-}$  dimer of those present in **1**. (Right): Said dimers upon assembly, participating in hydrogen bonds that go on to form chains down the *b*-axis.

At this stage, it is a bit unclear as to why this dimeric species is observed as similar preparations with related organic species in low pH, high anion media typically feature monomeric anions with H-bonding motifs between the equatorial chlorides and protonated N groups.<sup>2-4,10</sup> Also, preparations involving closely related substituted pyrazine have generated phases featuring protonated pyrazinium cations that hydrogen-bond to one another or to lattice halide anions.<sup>42</sup> One would expect the low pH environment to favor protonation over coordination, therefore one may speculate that a subtle balance of sterics and bond strengths may favor the formation of this dimer selectively, as we observe both protonation and coordination in the crystal structure of compound **1**.

## Spectroscopy

**UV-VIS-DRS Absorption Studies:** Compound **1** displays two strong bands with absorption edges about 400 nm and 490 nm, as shown in **SI Figure S2**. These bands are typical for uranyl containing compounds, and represent lower energy *axial*  $O_{yl} \rightarrow U$  ligand to metal charge transfer (LMCT), along with a higher energy equatorial LMCT.<sup>2,11,13</sup>

**Luminescence:** Solid state luminescence measurements were performed to serve as a secondary probe of the  $UO_2^{2+}$  coordination environment on electronic structure and bonding.<sup>3,10,43,44</sup> Compound **1** exhibits typical absorption and emission profiles at both room and low temperature, in which the band about 350 nm corresponds to the equatorial absorption, with the band at 420 nm due to the axial uranyl-oxo (**Figure 2**). The emission of **1** proceeds as a harmonic progression starting at *ca.* 500 nm, owing to a ligand to metal charge transfer (LMCT) from O-based molecular orbitals to U 5f atomic orbitals, which is typical for uranyl-bearing compounds. The splitting of these bands is due to coupling with equatorial ligands, which can also be seen in the calculated Raman videos (**SI GIFs 1 and 2**). The change in absorption profile from low to room temperature can be attributed to a decrease in non-radiative decay pathways of the pyrazine ring at low temperature, allowing for better absorption and therefore more radiative decay at low-temperature.

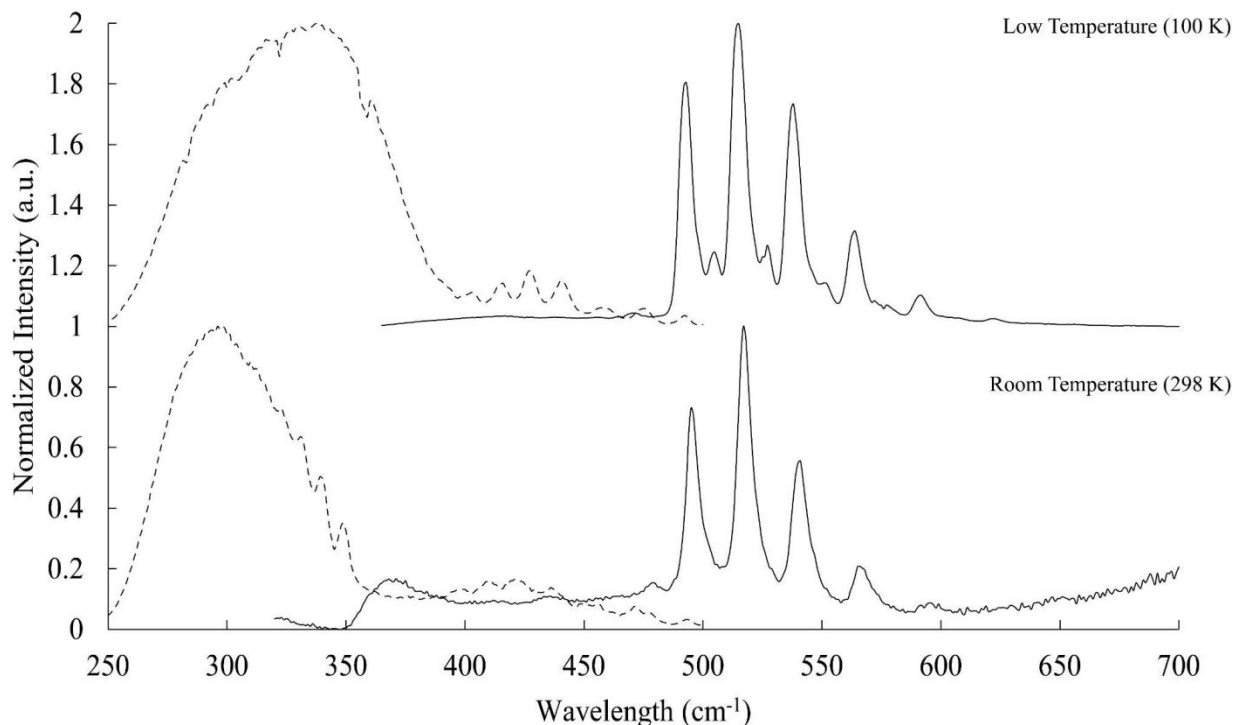


**Figure 2:** Room (bottom) and low-temperature (top) luminescence spectra (approximately 298 K and 100(2) K, respectively) of  $(\text{HPyz}^+)_2[\text{UO}_2\text{Cl}_3(\text{H}_2\text{O})(\text{Pyz})_{0.5}]_2 \cdot 2\text{H}_2\text{O}$

**Raman:** The uranium oxygen bond within the  $\text{UO}_2^{2+}$  unit is often probed *via* Raman spectroscopy, as it exhibits a strong, characteristic Raman-active symmetric stretching frequency ( $\nu_1$ ).<sup>11,13,43,44</sup> Changes in equatorial coordination, due to bonding or non-covalent interactions, are known to alter the frequency of this stretch, along with enhanced coordination to the uranyl oxygen. As the uranyl bond strengthens, we typically see a blue shift of  $\nu_1$ , meaning this value shifts to higher wavenumbers. Compound **1** has a  $\nu_1$  stretching frequency of  $862 \text{ cm}^{-1}$  (**SI Figure S3**) which indicates stronger  $\text{U}=\text{O}$  bonding than in corresponding  $[\text{UO}_2\text{Cl}_4]^{2-}$  units, which typically range from  $810\text{-}840 \text{ cm}^{-1}$ .

## Computational analysis

In order to rationalize assembly motifs present in **1**, as well as to understand the resultant impact on bonding, a rigorous computational analysis of both the  $[\text{UO}_2\text{Cl}_4]^{2-}$  monomer and  $[\text{UO}_2\text{Cl}_3(\text{H}_2\text{O})(\text{Pyz})_{0.5}]_2^{2-}$  dimer was performed. In doing so, we aim to understand changes to U=O bonding upon dimer formation, and inform future assembly efforts using this unit. Models were prepared using crystallographic atomic coordinates representing the  $[\text{UO}_2\text{Cl}_3(\text{H}_2\text{O})(\text{Pyz})_{0.5}]_2^{2-}$  dimer of compound **1** and the  $[\text{UO}_2\text{Cl}_4]^{2-}$  monomer (**SI Figures S4** and **S5**).<sup>3</sup>

**Calculated HOMO and LUMO:** Owing to the nature of electronic structure in molecular bridged complexes, we aimed to probe the composition of the HOMO and LUMO of the title compound, considering the potential for delocalization of the  $\pi$ -system across the pyrazine ligand. Our calculations indicate that our LUMO does, in fact, exhibit a highly delocalized  $\pi$  system across the pyrazine ligand and the  $\pi$  system of both uranyl centers (**Figure 3**). This is in contrast to the LUMO of compounds containing the  $[\text{UO}_2\text{Cl}_4]^{2-}$  anion, which exhibits a pure 5f orbital as its LUMO, shown in **SI Figure S7**, whereas the 5f orbitals of  $[\text{UO}_2\text{Cl}_3(\text{H}_2\text{O})(\text{Pyz})_{0.5}]_2^{2-}$  do not come into the electronic manifold until LUMO+1 and LUMO+2. This finding highlights the potential of this dimer to exhibit electron transfer and perhaps behave as other molecular bridged compounds, such as Creutz-Taube complexes.

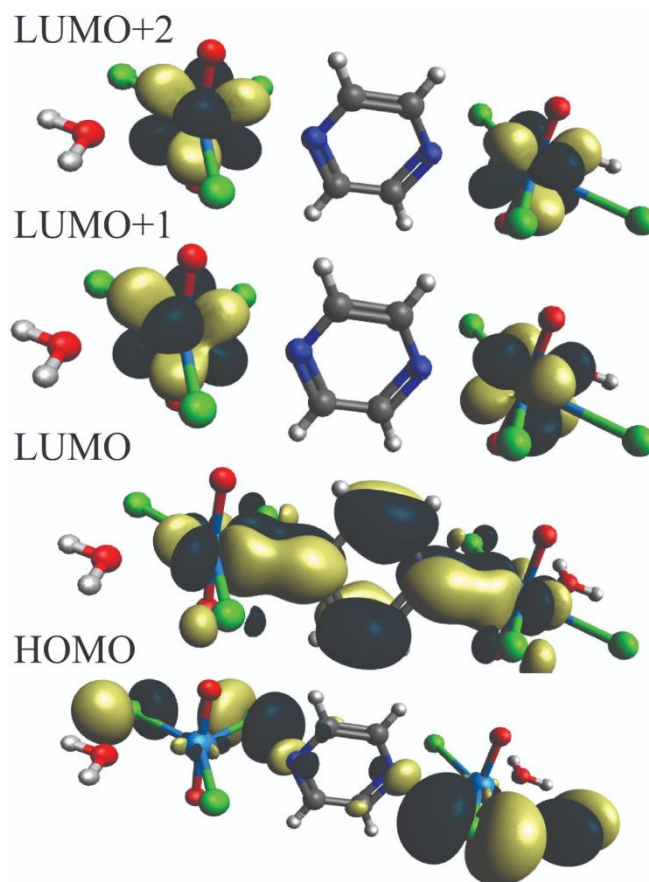


**Figure 3:** Isodensity representation of the HOMO/LUMO orbitals of  $[\text{UO}_2\text{Cl}_3(\text{H}_2\text{O})(\text{Pyz})_{0.5}]_2^{2-}$ , showing the delocalized LUMO, as well as the LUMO+1 and LUMO+2 composed of 5f character.

*Electrostatic surface potentials (ESPs):* Calculation and rendering of electrostatic potentials along a 0.002 au isosurface was done to evaluate candidate sites for non-covalent donor and acceptor sites on the anion. The best donor can be defined as the region where the potential is most positive, or in this (anionic) case, least negative. The best NCI donor site is the equatorial water, at -119.4 kJ/mol, with the best donor sites being the adjacent chlorides followed by the  $-\text{yl}$  oxo, at -601.7 kJ/mol and -569.3 kJ/mol, respectively (**Figure 4**). As the water and isolated chloride are adjacent to one another, it fits that these two atoms are responsible for the hydrogen bonding chains that form down the b-axis (**Figure 1**). One of the two remaining equatorial chlorides also participates in hydrogen bonding with lattice water molecules. Of note, the stark

decrease in electrostatic potential, and by extension basicity, of the uranyl in **1** with respect to  $[\text{UO}_2\text{Cl}_4]^{2-}$  suggests a lessened capacity to engage at the uranyl-oxo atoms.

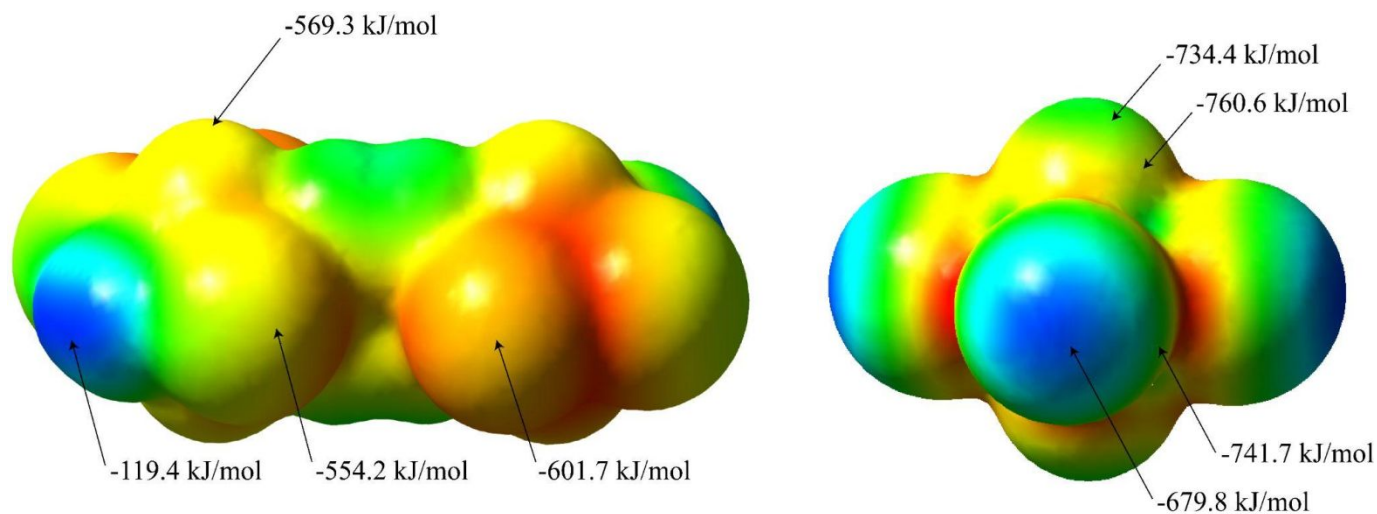


**Figure 4:** ESP of (Left):  $[\text{UO}_2\text{Cl}_3(\text{H}_2\text{O})(\text{Pyz})_{0.5}]_2^{2-}$  and (Right):  $[\text{UO}_2\text{Cl}_4]^{2-}$  at a 0.002 isosurface, highlighting the best donor/acceptor sites for second-sphere interactions on each anion.

**Frequency calculated vibrational modes.** Single point frequency calculations on both the monomeric  $[\text{UO}_2\text{Cl}_4]^{2-}$  and  $[\text{UO}_2\text{Cl}_3(\text{H}_2\text{O})(\text{Pyz})_{0.5}]_2^{2-}$  dimer are in agreement with observed Raman spectra. In the  $[\text{UO}_2\text{Cl}_4]^{2-}$  model, provided as **SI Table S4**, there is one Raman-active U=O symmetric stretching band predicted at  $862.61\text{ cm}^{-1}$ . The uranyl dimer, however, has a predicted symmetric stretching frequency, comprising the symmetric stretching mode of the coupled  $\text{UO}_2^{2+}$  centers, at  $870.31\text{ cm}^{-1}$  (**SI Figure S8**). In the experimental Raman spectra, there is one broad Raman band, likely due to the overlapping of this predicted band with pyrazine bending modes in this region. The relative blue shift in this band as compared to the typical monomer range, however, suggests stronger U=O bonding in the uranyl dimer.

**NBO analysis (NLMO and Wiberg Bond indices):** Natural Localized Molecular Orbital (NLMO) and Wiberg bond order analysis within NBO were used to probe the character,

composition, and strength of U=O bonds of **1**, in comparison to the  $[\text{UO}_2\text{Cl}_4]^{2-}$  monomer. NLMO calculations provide information regarding orbital composition and percent parent atom of specific bonds. For the purposes of comparing these two building units, a higher metal percent character in metal-ligand, or in this case, metal-oxygen and/or metal-chloride bonds, correlates to a stronger, more covalent bond between the two atoms. By extension, a higher Wiberg bond order correlates to stronger bonds as well.

By comparing the percent metal composition of U=O bonds between  $[\text{UO}_2\text{Cl}_3(\text{H}_2\text{O})(\text{Pyz})_{0.5}]_2^{2-}$  and  $[\text{UO}_2\text{Cl}_4]^{2-}$ , we observe a higher U% in both the  $\sigma$  and  $\pi$  bonds of the uranyl dimer, consistent with the predicted blue shift in both observed and calculated frequencies (**Table 1**, **SI Tables S3 and S4**). This, coupled with larger Wiberg bond indices for the U=O bonds of  $[\text{UO}_2\text{Cl}_3(\text{H}_2\text{O})(\text{Pyz})_{0.5}]_2^{2-}$  indicate that U=O bonds are stronger in the  $[\text{UO}_2\text{Cl}_3(\text{H}_2\text{O})(\text{Pyz})_{0.5}]_2^{2-}$  dimer (**Table 2**). Although we note an average increase in the U% of U-Cl bonds of  $[\text{UO}_2\text{Cl}_3(\text{H}_2\text{O})(\text{Pyz})_{0.5}]_2^{2-}$ , two of the three U-Cl values predict bond weakening (**Table 3**). This occurs in conjunction with almost no change in the average of Wiberg bond indices, again with two of three bonds suggesting U-Cl bond weakening.

**Table 1:** Percent parent atom composition of U=O  $\sigma$  and  $\pi$  bonds within the  $[\text{UO}_2\text{Cl}_3(\text{H}_2\text{O})(\text{Pyz})_{0.5}]_2^{2-}$  dimer and the  $[\text{UO}_2\text{Cl}_4]^{2-}$  anion.

	$\sigma$		$\pi$	
	U%	O%	U%	O%
$[\text{UO}_2\text{Cl}_3(\text{H}_2\text{O})(\text{Pyz})_{0.5}]_2^{2-}$	28.424	70.000	21.418	78.385
$[\text{UO}_2\text{Cl}_4]^{2-}$	28.310	68.564	21.250	78.518

**Table 2:** Calculated Wiberg bond indices of first sphere metal-ligand bonds within the  $[\text{UO}_2\text{Cl}_3(\text{H}_2\text{O})(\text{Pyz})_{0.5}]_2^{2-}$  dimer and the  $[\text{UO}_2\text{Cl}_4]^{2-}$  anion.

Atom 1-Atom 2	$[\text{UO}_2\text{Cl}_3(\text{H}_2\text{O})(\text{Pyz})_{0.5}]_2^{2-}$	$[\text{UO}_2\text{Cl}_4]^{2-}$
U-O1	2.0695	2.0540
U-O2	2.0645	2.0540
Average U=O	2.0670	2.0540
U-Cl1	0.7663	0.8235
U-Cl2	0.8575	0.8424
U-Cl3	0.8749	0.8237
U-Cl4	-	0.8415
Average U-Cl	0.8329	0.8328
U-OH <sub>2</sub>	0.3157	-
U-N1	0.3247	-

**Table 3:** Percent parent atom composition of the U-Cl bonds within  $[\text{UO}_2\text{Cl}_3(\text{H}_2\text{O})(\text{Pyz})_{0.5}]_2^{2-}$  dimer and the  $[\text{UO}_2\text{Cl}_4]^{2-}$  anion.

Bond	$[\text{UO}_2\text{Cl}_3(\text{H}_2\text{O})(\text{Pyz})_{0.5}]_2^{2-}$		$[\text{UO}_2\text{Cl}_4]^{2-}$	
	%U	%Cl	%U	%Cl
U-Cl1	13.801	85.115	14.163	85.562
U-Cl2	13.335	85.165	14.279	85.440
U-Cl3	15.983	83.537	14.144	85.572
U-Cl4	-	-	14.273	85.445
Average U-Cl	14.373	84.606	14.215	85.505

**QTAIM metrics of uranyl-ligand bonding:** QTAIM metrics may also be seen as further evidence of the strengthening of actinide-ligand bonds within  $[\text{UO}_2\text{Cl}_3(\text{H}_2\text{O})(\text{Pyz})_{0.5}]_2^{2-}$  with respect to  $[\text{UO}_2\text{Cl}_4]^{2-}$ . Previous work by Platts and Baker detailed metrics to evaluate bond critical points, type, and order. Key metrics include bond density at critical points ( $\rho$ ), as well as the magnitude of the Laplacian of bond density ( $\nabla^2\rho$ ), total energy density ( $H$ ), and delocalization index ( $D_{(A|B)}$ ). Higher electron density at a bond critical point correlates to a higher bond order,

and by extension, stronger bonding. A positive increase in total energy density, in conjunction with increased magnitude of the Laplacian and delocalization are also indicative of stronger metal ligand bonding.<sup>45</sup>

In the case of  $[\text{UO}_2\text{Cl}_3(\text{H}_2\text{O})(\text{Pyz})_{0.5}]_2^{2-}$ , we note increased energy density of the bond critical point in U=O bonds versus those in  $[\text{UO}_2\text{Cl}_4]^{2-}$ . This metric is also supported by increases in the magnitude of both the Laplacian and delocalization indices for the U=O bonds. For U-Cl bonds, however, we note decreases in these values, in conjunction with previous metrics, for  $[\text{UO}_2\text{Cl}_3(\text{H}_2\text{O})(\text{Pyz})_{0.5}]_2^{2-}$  which predicts weaker, less ionic bonding.

**Table 4:** QTAIM metrics for  $[\text{UO}_2\text{Cl}_3(\text{H}_2\text{O})(\text{Pyz})_{0.5}]_2^{2-}$  and  $[\text{UO}_2\text{Cl}_4]^{2-}$ .

	$\rho$	$\nabla^2\rho$	$\epsilon$	V	G	H	D(A B)
<b><math>[\text{UO}_2\text{Cl}_3(\text{H}_2\text{O})(\text{Pyz})_{0.5}]_2^{2-}</math></b>							
U1 - O1	0.310527	0.312041	0.014525	-0.642574	0.360282	-0.282292	1.902679
U1 - O2	0.311455	0.312849	0.011951	-0.646401	0.362296	-0.284105	1.896862
Average U=O	0.310991	0.312445	0.013238	-0.644488	0.361289	-0.283199	1.899771
U1 - Cl1	0.053431	0.117402	0.084730	-0.047191	0.038271	-0.008920	0.482761
U1 - Cl2	0.058527	0.124139	0.092812	-0.053153	0.042094	-0.011059	0.569888
U1 - Cl3	0.060436	0.133402	0.112329	-0.056772	0.045062	-0.011710	0.556707
Average U-Cl	0.057465	0.124981	0.096624	-0.052372	0.041809	-0.010563	0.536452
U1 - O3	0.055081	0.219886	0.252841	-0.061474	0.058223	-0.003251	0.263313
U1 - N1	0.049815	0.133882	0.084201	-0.044149	0.038810	-0.005339	0.280189
<b><math>[\text{UO}_2\text{Cl}_4]^{2-}</math></b>							
U1 - O1	0.306099	0.319235	0.000814	-0.628149	0.353970	-0.274179	1.889761
U1 - O2	0.306045	0.319272	0.000815	-0.627966	0.353883	-0.274083	1.889779
Average U=O	0.306072	0.319254	0.000815	-0.628058	0.353927	-0.274131	1.889770
U1 - Cl1	0.060881	0.137784	0.048336	-0.057788	0.046117	-0.011671	0.565430
U1 - Cl2	0.063143	0.142800	0.047968	-0.060939	0.048319	-0.012620	0.581146
U1 - Cl3	0.060909	0.137854	0.048365	-0.057829	0.046146	-0.011683	0.565569
U1 - Cl4	0.063026	0.142499	0.047838	-0.060763	0.048194	-0.012569	0.580435
Average U-Cl	0.061990	0.140234	0.048127	-0.059330	0.047194	-0.012136	0.573145

## Conclusions

We have prepared a novel symmetric pyrazine bridged uranyl dimer, which may serve as a model for future actinyl-bearing complexes of this type. Our study has shown that changing first sphere coordination from the typical  $[\text{UO}_2\text{Cl}_4]^{2-}$  dianion to the  $[\text{UO}_2\text{Cl}_3(\text{H}_2\text{O})(\text{Pyz})_{0.5}]_2^{2-}$  dimer dramatically delocalizes the uranyl axial  $\pi$ -system across the equatorial pyrazine ligand. Concurrent with the observed delocalization, we note a strengthening of U=O bonds, relative to the  $[\text{UO}_2\text{Cl}_4]^{2-}$  monomer. This bond strengthening is reflected in a drastic increase in the ESP of the uranyl oxygen, a blue shift in the Raman shift compared to typical  $[\text{UO}_2\text{Cl}_4]^{2-}$  bearing materials, and increased U% in U=O bond composition. As U=O bonds within the uranyl strengthen, and therefore become less Lewis basic, this species may be less apt to form oxo interactions. Nevertheless, complexes of this type may be promising targets for future mixed-valent and/or bimetallic actinyl compounds capable of electron transfer in future efforts.

## Associated Content

### Electronic Supporting Information

The Electronic Supporting Information is available free of charge on the RSC website. Crystallographic information on CCDC 2169103 can be obtained free of charge by e-mailing [data\\_request@ccdc.cam.ac.uk](mailto:data_request@ccdc.cam.ac.uk) or by contacting The Cambridge Crystallographic Data Centre, 12 Union Road, Cambridge, CB2 1EZ UK; Fax +44(0)1223-336033; [http://www.ccdc.cam.ac.uk/data\\_request/cif](http://www.ccdc.cam.ac.uk/data_request/cif).

Crystallography tables, experimental Raman and UV-Vis-DRS spectra, and computational details for the  $[\text{UO}_2\text{Cl}_4]^{2-}$  and  $[\text{UO}_2\text{Cl}_3(\text{H}_2\text{O})(\text{Pyz})_{0.5}]_2^{2-}$  models, and method validation tables. (PDF)  
Video of atomic displacement for Raman stretches in  $[\text{UO}_2\text{Cl}_3(\text{H}_2\text{O})(\text{Pyz})_{0.5}]_2^{2-}$  at  $878\text{ cm}^{-1}$  (GIFs 1 and 2)

Video of atomic displacement for Raman stretch in  $[\text{UO}_2\text{Cl}_3(\text{H}_2\text{O})(\text{Pyz})_{0.5}]_2^{2-}$  at  $882\text{ cm}^{-1}$   
(**GIF 3**)  
X-ray data for compound **1** (CIF)

### Author Information

**\*Christopher L. Cahill** - Department of Chemistry, The George Washington University, Washington, DC 20052, United States; [orcid.org/0000-0002-2015-3595](https://orcid.org/0000-0002-2015-3595);  
Email: [cahill@gwu.edu](mailto:cahill@gwu.edu)

### Authors

**Nicole M. Byrne** - Department of Chemistry, The George Washington University, Washington, DC 20052, United States; [orcid.org/0000-0003-0553-5373](https://orcid.org/0000-0003-0553-5373);  
Email: [nbyrne@gwu.edu](mailto:nbyrne@gwu.edu)

**Mark H. Schofield** - Department of Chemistry, The George Washington University, Washington, DC 20052, United States; [orcid.org/0000-0002-9601-7186](https://orcid.org/0000-0002-9601-7186);  
Email: [mschofie@gwu.edu](mailto:mschofie@gwu.edu)

### Conflicts of Interest

There are no conflicts to declare.

### Acknowledgements

This study was supported by the U.S. Department of Energy (DOE) – Chemical Sciences, Geosciences, and Biosciences Division, Office of Science, Office of Basic Energy Sciences, Heavy Elements Program, under grant number DE-FG02-05ER15736. We gratefully acknowledge the computing resources provided by the High-Performance Computing Cluster operated by Research Technology Services at the George Washington University. The authors would also like

to thank Professor Karah Knope and Alexander Marwitz of Georgetown University for providing Raman microscope time.

## References

1. Carter KP, Surbella RG, Kalaj M, Cahill CL. Restricted Speciation and Supramolecular Assembly in the 5f Block. *Chemistry – A European Journal*. 2018;24(49):12747–56.
2. Surbella RG, Ducati LC, Pellegrini KL, McNamara BK, Autschbach J, Schwantes JM, et al. Transuranic Hybrid Materials: Crystallographic and Computational Metrics of Supramolecular Assembly. *J Am Chem Soc*. 2017 Aug 9;139(31):10843–55.
3. Surbella RG, Andrews MB, Cahill CL. Self-assembly of  $[\text{UO}_2\text{X}_4]^{2-}$  ( $\text{X}=\text{Cl}, \text{Br}$ ) dianions with  $\gamma$  substituted pyridinium cations: Structural systematics and fluorescence properties. *Journal of Solid State Chemistry*. 2016 Apr;236:257–71.
4. Deifel NP, Cahill CL. The uranyl tetrachloride anion as a tecton in the assembly of U(VI) hybrid materials. *CrystEngComm*. 2009 Nov 16;11(12):2739–44.
5. Pyrch MM, Williams JM, Kasperski MW, Applegate LC, Forbes TZ. Synthesis and spectroscopic characterization of actinyl(VI) tetrahalide coordination compounds containing 2, 2'-bipyridine. *Inorganica Chimica Acta*. 2020 Aug 1;508:119628.
6. de Groot J, Gojdas K, Unruh DK, Forbes TZ. Use of Charge-Assisted Hydrogen Bonding in the Supramolecular Assembly of Hybrid Uranyl Materials. *Crystal Growth & Design*. 2014 Mar 5;14(3):1357–65.
7. Oher H, Réal F, Vercoouter T, Vallet V. Investigation of the Luminescence of  $[\text{UO}_2\text{X}_4]^{2-}$  ( $\text{X} = \text{Cl}, \text{Br}$ ) Complexes in the Organic Phase Using Time-Resolved Laser-Induced Fluorescence Spectroscopy and Quantum Chemical Simulations. *Inorg Chem*. 2020 May 4;59(9):5896–906.
8. Lhoste J, Henry N, Loiseau T, Guyot Y, Abraham F. Crystal structures of 2,2':6',2''-terpyridine uranyl chlorides molecular assemblies and their luminescence signatures. *Polyhedron*. 2013 Feb 13;50(1):321–7.
9. Li F ze, Mei L, Hu K qiu, An S wen, Wu S, Liu N, et al. Uranyl Compounds Involving a Weakly Bonded Pseudorotaxane Linker: Combined Effect of pH and Competing Ligands on Uranyl Coordination and Speciation. *Inorg Chem*. 2019 Mar 4;58(5):3271–82.

10. Andrews MB, Cahill CL. Uranyl Bearing Hybrid Materials: Synthesis, Speciation, and Solid-State Structures. *Chem Rev.* 2013 Feb 13;113(2):1121–36.
11. Lu G, Haes AJ, Forbes TZ. Detection and identification of solids, surfaces, and solutions of uranium using vibrational spectroscopy. *Coordination Chemistry Reviews.* 2018 Nov 1;374:314–44.
12. Sergentu DC, Gendron F, Walter ED, Park S, Capan C, Surbella RG, et al. Equatorial Electronic Structure in the Uranyl Ion: Cs<sub>2</sub>UO<sub>2</sub>Cl<sub>4</sub> and Cs<sub>2</sub>UO<sub>2</sub>Br<sub>4</sub>. *Inorg Chem.* 2022 Mar 7;61(9):3821–31.
13. Pyrch MM, Williams JM, Kasperski MW, Applegate LC, Forbes TZ. Synthesis and spectroscopic characterization of actinyl(VI) tetrahalide coordination compounds containing 2, 2'-bipyridine. *Inorganica Chimica Acta.* 2020 Aug;508:119628.
14. Creutz Carol, Taube H. Binuclear complexes of ruthenium amines. *J Am Chem Soc.* 1973 Feb;95(4):1086–94.
15. Fuerholz U, Joss S, Buergi HB, Ludi A. The Creutz-Taube complex revisited: crystallographic study of the electron-transfer series (μ-pyrazine)decaamminediruthenium ([ $(\text{NH}_3)_5\text{Ru}(\text{Pyz})\text{Ru}(\text{NH}_3)_5$ ]<sup>n+</sup> (n = 4-6)). *Inorg Chem.* 1985 Mar 1;24(6):943–8.
16. Wong KY, Schatz PN. Resonance raman calculations in mixed-valence systems. Wolfram's red and the creutz-taube complex. *Chemical Physics Letters.* 1980 Aug 1;73(3):456–60.
17. Taube H, Myers H. Evidence for a Bridged Activated Complex for Electron Transfer Reactions. *J Am Chem Soc.* 1954 Apr;76(8):2103–11.
18. da Silva AR, de Almeida JS, Rivelino R. A Theoretical Assessment of Spin and Charge States in Binuclear Cobalt–Ruthenium Complexes: Implications for a Creutz–Taube Model Ion Separated by a C60-Derivative Bridging Ligand. *J Phys Chem A.* 2020 Dec 24;124(51):10826–37.
19. Todorova T, Delley B. The Creutz–Taube Complex Revisited: DFT Study of the Infrared Frequencies. *Inorg Chem.* 2008 Dec 1;47(23):11269–77.
20. Mehdoui T, Berthet JC, Thuéry P, Ephritikhine M. Clear-Cut Lanthanide(III)/Actinide(III) Differentiation in Coordination of Pyrazine to Tris(cyclopentadienyl) Complexes of Cerium and Uranium, Involving Reversible U<sup>III</sup> → U<sup>IV</sup> Oxidation. *European Journal of Inorganic Chemistry.* 2004;2004(10):1996–2000.
21. Bruker. APEX III. Madison, Wisconsin, USA: Bruker AXS Inc.; 2020.
22. Bruker. SAINT. Madison, Wisconsin, USA: Bruker AXS Inc.; 2020.

23. Lubben J, Wandtke CM, Hubschle CB, Ruf M, Sheldrick, G. M. , Aspherical Scattering Factors for SHELXL – Model, Implementation and Application. *Acta Cryst A: Found Adv.* 2019;(78):50–62.
24. Sheldrick GM. A short history of SHELX. *Acta Crystallogr A.* 2008 Jan;64(Pt 1):112–22.
25. Farrugia LJ. WinGX and ORTEP for Windows: an update. *J Appl Crystallogr.* 2012;(45):849–54.
26. Palmer DC. CrystalMaker 8.2.2. Begbroke, Oxfordshire, England: CrystalMaker Software Ltd.; 2014.
27. Frisch MJ, Trucks GW, Schlegel HB, Scuseria GE, Robb MA, Cheeseman JR, et al. *Gaussian 16 Rev. C.01.* Wallingford, CT; 2016.
28. Glendening ED, Badenhoop JK, Reed AE, Carpenter JE, Bohmann JA, Morales CM, et al. *NBO 7.0.* University of Wisconsin-Madison: Theoretical Chemistry Institute; 2018.
29. Glendening ED, Landis CR, Weinhold F. Natural Bond Orbital Methods. *WIREs Comput Mol Sci.* 2012;(2):1–42.
30. Weinhold F, Landis CR. Natural Bonding Orbitals and Extensions of Localized Bonding Concepts. *Chem Educ Res Pract.* 2001;(2):91–104.
31. Cao X, Dolg M. Segmented Contraction Scheme for Small-Core Actinide Pseudopotential Basis Sets. *J Molec Struct (Theochem).* 2004;(673):203.
32. Cao X, Dolg M, Stoll H. Valence Basis Sets for Relativistic Energy-Consistent Small-Core Actinide Pseudopotentials. *J Chem Phys.* 2003;(118):487.
33. Grimme S, Ehrlich S, Goerigk L. Effect of the damping function in dispersion corrected density functional theory. *Journal of Computational Chemistry.* 2011;32(7):1456–65.
34. Grimme S, Antony J, Ehrlich S, Krieg H. A consistent and accurate ab initio parametrization of density functional dispersion correction (DFT-D) for the 94 elements H-Pu. *J Chem Phys.* 2010 Apr 21;132(15):154104.
35. Dennington R, Keith TA, Millam JM. *GaussView.* Shawnee Mission, KS: Semichem Inc; 2016.
36. Hanwell MD, Curtis DE, Lonie DC, Vandermeersch T, Zurek E, Hutchison GR. Avogadro: An Advanced Semantic Chemical Editor, Visualization, and Analysis Platform. *J Cheminf.* 2012;(4).
37. Avogadro: An Open-source Molecular Builder and Visualization Tool [Internet]. Available from: <http://avogadro.cc/>

38. Bader RFW, Nguyen-Dang TT. Quantum Theory of Atoms in Molecules–Dalton Revisited. In: Löwdin PO, editor. *Advances in Quantum Chemistry* [Internet]. Academic Press; 1981 [cited 2021 Aug 15]. p. 63–124. Available from: <https://www.sciencedirect.com/science/article/pii/S0065327608603263>
39. Keith TA. AIMAll [Internet]. Overland Park KS, USA: Gristmill Software; 2019. Available from: [aim.tkgristmill.com](http://aim.tkgristmill.com)
40. KUMAR PSV, RAGHAVENDRA V, SUBRAMANIAN V. Bader's Theory of Atoms in Molecules (AIM) and its Applications to Chemical Bonding. *J Chem Sci.* 2016 Oct 1;128(10):1527–36.
41. Bondi A. van der Waals Volumes and Radii. *J Phys Chem.* 1964 Mar;68(3):441–51.
42. Byrne NM, Cahill CL. A structural and spectroscopic investigation of structure-property relationships in systematic hybrid [UO<sub>2</sub>X<sub>4</sub>]<sup>2-</sup> (X= Cl, Br) bearing materials. In Preparation. 2022;
43. Carter KP, Kalaj M, Surbella III RG, Ducati LC, Autschbach J, Cahill CL. Engaging the Terminal: Promoting Halogen Bonding Interactions with Uranyl Oxo Atoms. *Chemistry – A European Journal.* 2017;23(61):15355–69.
44. Byrne N, Nicholas A, Schofield M, Cahill C. Bimetallic uranyl/cobalt(ii) isothiocyanates: structure, property and spectroscopic analysis of homo- and heterometallic phases. *Dalton Trans.* 2021;(26):9158–72.
45. Baker RJ, Platts JA. A computational investigation of orbital overlap versus energy degeneracy covalency in [UE<sub>2</sub>]<sup>2+</sup> (E = O, S, Se, Te) complexes | EndNote Click [Internet]. [cited 2022 Apr 5]. Available from: [https://click.endnote.com/viewer?doi=10.1039%2F04484a&token=WzIwNzc0NjAsIjEwLjEwMzkvYzlkDA0NDg0YSJd.1yLUD6\\_mFvVV-J96iq4IM9Lks\\_E](https://click.endnote.com/viewer?doi=10.1039%2F04484a&token=WzIwNzc0NjAsIjEwLjEwMzkvYzlkDA0NDg0YSJd.1yLUD6_mFvVV-J96iq4IM9Lks_E)